Pergamon

Int. J. Heat Mass Transfer. Vol. 40, No. 1, pp. 141–147, 1997
Copyright © 1996 Elsevier Science Ltd
Printed in Great Britain. All rights reserved
0017-9310/97 $15.00+0.00

PII: S0017-9310(96)00086-5

Numerical investigation of heat transfer in impinging axial and radial jets with superimposed swirl

B. L. OWSENEK, T. CZIESLA, N. K. MITRA† and G. BISWAS‡

Institut für Thermo- und Fluiddynamik, Ruhr-Universität Bochum, Bochum, Germany

(*Received* 8 *August* 1995 *and in final form* 26 *January* 1996)

Abstract—The effect of swirl on heat transfer by axial and radial laminar jets impinging on a flat plate has been investigated numerically through the solution of Navier–Stokes and energy equations. Heat transfer is reduced substantially by the superposition of swirl on axial jets. Significant enhancement in heat transfer has been observed in the case of a radial jet with superimposed swirl on it. For a swirl number of unity, the heat transfer is enhanced by 77%. Copyright © 1996 Elsevier Science Ltd.

INTRODUCTION

Impinging jets are commonly used in many industrial applications to enhance heat or mass transfer from the impingement surface. In typical engineering applications, such jets are usually turbulent and arranged in banks to produce high transfer coefficients over an extended area. Most engineering applications use an impinging axial jet (Fig. 1), which produces high transfer coefficients with a relatively low pressure drop. In a recent review paper Viskanta [1] presents the state of knowledge on heat transfer by impinging jets. In recent years, the radial jet (Fig. 2) has received increased academic attention and found industrial application due to its ability to produce moderately high transfer rates over a large area, while producing a net force on the impingement surface which may be positive, negative or zero.

In radial jets, flow discharges from the side of the feed tube, then curves down and attaches to the impingement surface due to the Coanda effect. Moderately high transfer coefficients are found on the reattachment ring. Heat transfer coefficients drop outside the impingement ring, where a wall jet develops. Relatively low heat transfer coefficients are also found in the recirculation region under the feed tube [2].

Performance of radial and impinging jets can be varied through manipulation of various geometrical and flow parameters. The pertinent geometrical parameters in the case of an axial jet are the nozzle exit height and diameter. The radial jet possesses two additional parameters, viz, the exit angle and the discharge width. Furthermore, the parameters, such as, Reynolds number, Prandtl number, Grashof number, entrance profile and entrance swirl have an effect on the resultant flowfield and the transport coefficients. In particular, swirl is an interesting parameter, because it is independent of the mass flow rate; consequently, massflow limited systems can benefit directly from swirl-induced transport enhancement.

Swirl is generally quantified by swirl number which is defined as angular momentum flux divided by axial momentum flux and jet diameter

$$S = \frac{G_\theta}{G_x(2R)}. \tag{1}$$

As the swirl number is increased in an axial jet, the rate of entrainment from the surroundings, the radial extent of the jet and the decay rate of the axial velocity are increased. In a free axial jet, even a weak swirl can

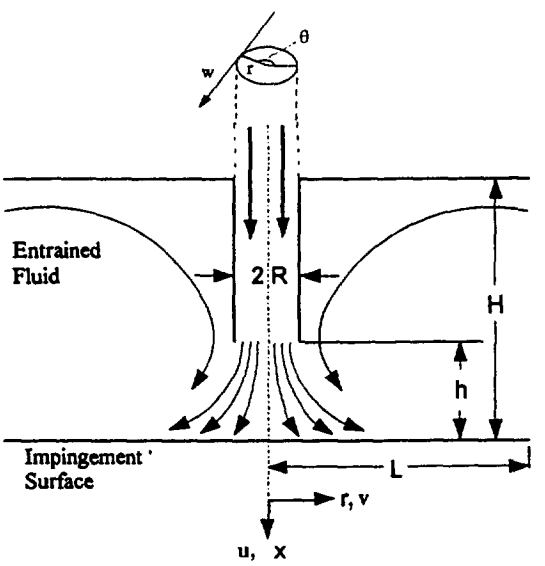

Fig. 1. Axial jet.

† Author to whom correspondence should be addressed.
‡ Current address: Indian Institute of Technology, Kanpur-208016, India.

NOMENCLATURE

c_f	friction factor	t	dimensionless time
G	momentum flux [kg m s^{-2}]	T	dimensionless temperature
h	dimensionless jet height from the impingement plate	u	dimensionless velocity component in x-direction
H	dimensionless height of the enclosing wall	v	dimensionless velocity component in r-direction
L	dimensionless radius of the impingement plate	w	dimensionless velocity component in θ-direction
Nu_r	local Nusselt number, equation (7)	u_{in}	entrance velocity [m s^{-1}]
P	dimensionless pressure	x	axial coordinate.
p_{sr}	dimensionless local surface pressure		
p_s	dimensionless average surface pressure	Greek symbols	
Pr	Prandtl number	ν	dynamic viscosity [m^2 s^{-1}]
r	radial coordinate	ρ	density [kg m^{-3}]
R	radius of the feed tube [m]	θ	azimuthal coordinate
Re	Reynolds number	ϑ	jet exit angle
S	swirl number, equation (1)	ω	angular velocity [rad s^{-1}].

induce an adverse pressure gradient and decrease the axial velocity [3]

Huang *et al.* [4] have performed a parametric numerical study of partially confined laminar jets with swirl and they have concluded that swirl encourages recirculation, thereby decreasing transport coefficients. Additionally, they note that swirl below $S = 0.2$ has very little effect on the flow field or transport rate.

An experimental study by Ward and Mahmood [5] has found that swirl can strongly affect the nature of the local heat transfer coefficients in the impingement region, eliminating and smoothing the characteristic two-peak distribution with swirl as low as $S = 0.24$. At higher swirl numbers, the heat transfer at the impingement point is severely depressed, with the heat transfer peak occuring at a nondimensional location between 1.5 and 2. Most importantly, however, imposed swirl is found to reduce the overall heat transfer at all jet heights and Reynolds numbers of interest. They present a Nusselt number correlation which predicts a reduction of the average heat transfer according to $(1-S)^{0.57}$ for $S < 0.48$.

A more recent paper by the same authors [6] examines the effect of swirl in a rectangular nozzle array. In this case, interaction between neighboring co-rotating jets leads to an overall heat transfer enhancement. Such an enhancement has been observed only at intermediate swirl numbers ($0.12 < S < 0.24$) when the nozzle array is relatively close to the impingement surface. Nevertheless, the positive results recorded by these authors suggest that swirl deserves further attention.

The goal of this work is to examine the two-dimensional axisymmetric flow fields of impinging radial and axial jets, with a focus on the effects of superimposed swirl at the entrance. As such jets are used in industry to enhance transport rates, we investigate local and average Nusselt numbers in order to identify performance trends that could aid in optimization efforts. Because the principal advantage of the radial jets is the ability to control the surface normal force, we also examine the effects of entrance swirl on the surface pressure. However, we investigate here radial jets discharging parallel to the impingement surface, i.e. radial jets with 0° exit angle.

The complete near and far-field flow structure and temperature fields can be simulated by solving the unsteady Navier–Stokes and energy equations. In this work we consider the laminar flow behavior in the flow regime where the flow becomes periodic and, later, unsteady aperiodic. Since the overall structure of such low-Reynolds number flows should be quali-

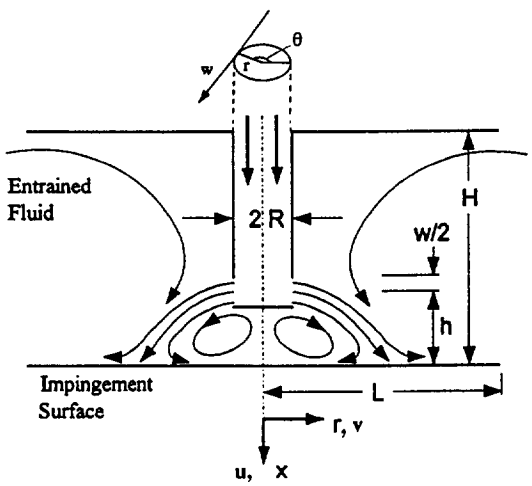

Fig. 2. Radial jet.

tatively similar to that found in the fully turbulent cases, the trends observed in this work should have a broad industrial significance.

COMPUTATION SCHEME

The Navier–Stokes and energy equations for incompressible flows have been solved in non-dimensional form with constant properties. Effect of free convection has been neglected here. In cylindrical coordinates the nondimensional equations with rotational symmetry are:

continuity equation

$$\frac{\partial u}{\partial x}+\frac{1}{r}\left(\frac{\partial}{\partial r}rv\right)=0; \tag{2}$$

axial momentum equation

$$\frac{\partial u}{\partial t}+\frac{\partial u^2}{\partial x}+\frac{\partial(ruw)}{r\,\partial r}=-\frac{\partial P}{\partial x}+\frac{1}{Re}\left[\frac{\partial^2 u}{\partial x^2}+\frac{\partial}{r\,\partial r}\left(r\frac{\partial u}{\partial r}\right)\right]; \tag{3}$$

radial momentum equation

$$\frac{\partial v}{\partial t}+\frac{\partial(uv)}{\partial x}+\frac{\partial(rv^2)}{r\,\partial r}-\frac{w^2}{r}=-\frac{\partial P}{\partial r}+\frac{1}{Re}\left[\frac{\partial^2 v}{\partial x^2}+\frac{\partial}{\partial r}\left(\frac{\partial}{r\,\partial r}(rv)\right)\right]; \tag{4}$$

circumferential momentum equation

$$\frac{\partial w}{\partial t}+\frac{\partial(uw)}{\partial x}+\frac{\partial(rvw)}{r\,\partial r}=+\frac{1}{Re}\left[\frac{\partial^2 w}{\partial x^2}+\frac{\partial}{\partial r}\left(\frac{\partial(rw)}{r\,\partial r}\right)\right]; \tag{5}$$

energy equation

$$\frac{\partial T}{\partial t}+\frac{\partial(uT)}{\partial x}+\frac{\partial(rvT)}{r\,\partial r}=\frac{1}{Re\,Pr}\left[\frac{\partial^2 T}{\partial x^2}+\frac{\partial}{r\,\partial r}\left(r\frac{\partial T}{\partial r}\right)\right]. \tag{6}$$

The equations have been nondimensionalized with the variables $u=\boldsymbol{u}/\boldsymbol{u}_{\text{in}}$, $v=\boldsymbol{v}/\boldsymbol{u}_{\text{in}}$, $w=\boldsymbol{w}/\boldsymbol{u}_{\text{in}}$, $P=\boldsymbol{P}/\boldsymbol{u}_{\text{in}}^2$, $T=\boldsymbol{T}/\boldsymbol{T}_\infty$, $x=\boldsymbol{x}/\boldsymbol{R}$, $r=\boldsymbol{r}/\boldsymbol{R}$, where bold italicized variables represent dimensional values and T_∞ is the ambient temperature. Nondimensional parameters such as Re and Pr are based on the standard definitions with $\boldsymbol{u}_{\text{in}}$ as the velocity parameter. Note that $\boldsymbol{u}_{\text{in}}$ is defined as the average velocity at the jet exit, based on volume flow rate.

The equations have been discretized in time using the Adams–Bashforth approach. Spatial derivatives are arranged on a staggered grid, with pressure and temperature at the center node and velocity components on the cell faces. Convection and diffusion have been linked using a flux-blending scheme with central and upwind components, in order to minimize numerical diffusion and assure numerical stability. The discretized equations are then solved using a fractional time step method of Kim and Moin [7].

A computational mesh with 30×42 grids (in x- and r-directions, respectively) was used. Grid spacing was reduced near the impingement plate to improve Nusselt number accuracy. This facilitated the computation of several geometries under myriad, unsteady conditions. Despite the relative roughness of the grid, the results showed only minor variation with grid refinement. For example, for an axial jet with a Reynolds number of 500, the average Nusselt number due to (30×42) grids varied by only 0.013% from that of the 52×82 grids, and 0.6% from that of the 100×162 grids.

The exit plane of the computational domain ($x=L$ and $r=H$ in Figs. 1 and 2) has been modeled with the assumption of constant pressure. The velocity at the exit plane is therefore modeled using mass continuity in the normal direction. In the tangential direction the efflux velocity gradient has been assumed to be zero. For the consistancy of the fractional time-step, intermediate boundary conditions are employed through the use of the method advocated by Kim and Moin [7].

All surfaces, with the exception of the constant-temperature impingement plane, have been assumed adiabatic. The impingement surface is maintained at $T_s=\eta T_\infty$, where η is greater than unity and can be varied following the requirement of the physical situation. The surroundings and fluid issuing from the jet are modeled with $T=T_\infty$. A Prandtl number of 0.72 has been used, which corresponds to room-temperature air. A temperature gradient of zero is used for flow efflux at the out flow plane of the computational domain.

RESULTS AND DISCUSSION

Computations have been performed for radial and axial jets in air ($Pr=0.72$) for various Reynolds numbers which varied between 10 and 1000. At low Reynolds numbers, steady solutions are obtained. However, as the Reynolds number is increased, first periodic, then chaotically unsteady solutions, are observed. No attempt has been made in this work to identify the transition points between the different regimes, as previous work by Huang *et al.* [2] has examined this question in a similar geometry.

From the computed temperature field, local Nusselt number on the impingement plate has been calculated based on the formula

$$Nu_r=\frac{\boldsymbol{T}_\infty}{(\boldsymbol{T}_s-\boldsymbol{T}_\infty)}\frac{\partial T}{\partial x}\bigg|_{x=0}. \tag{7}$$

Similarly, from the velocity field, the local coefficient of friction has been calculated according to

$$c_{\text{fr}}=\frac{1}{2Re}\frac{\partial v}{\partial x}\bigg|_{x=0}. \tag{8}$$

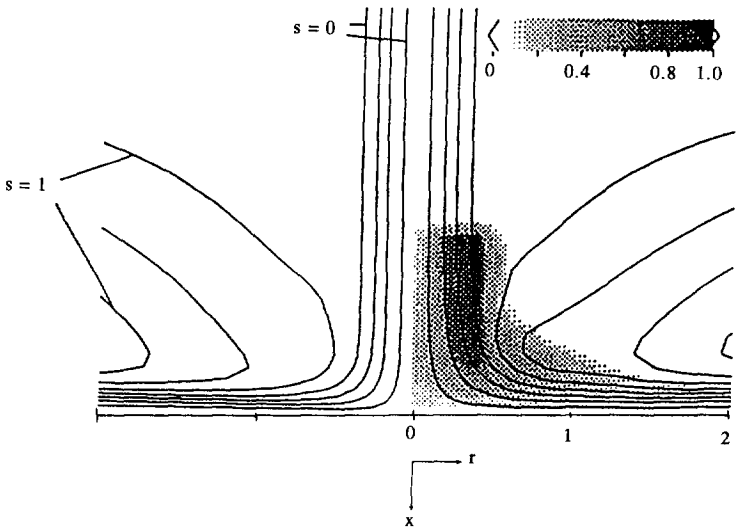

Fig. 3. Axial jet streamlines for $S = 0$ and $S = 1$ at $Re = 500$. Shading contours indicate circumferential velocity.

Note that the friction coefficient, as defined here, is actually the component of the friction coefficient in the radial direction. In addition, it should be recognized that the unsteady nature of the solutions obtained in this study required time-averaging to yield appropriate values.

Axial jet with swirl

The axial jet geometry considered in this study has a nondimensional radius of 0.5, an exit at 1.25 nondimensional units above the impingement surface, and is located in a partially enclosed cavity of height (H) 3 and radius (L) 5. As previous work by Laschefski *et al.* [8] has shown that the effect of the entrance velocity profile on the resultant heat transfer is relatively small, a parabolic entrance velocity profile is assumed.

A simplistic solid-body rotational profile has been assumed at the jet exit, such that $w = r\omega$. The swirl number has been varied between 0 and 1 at Reynolds numbers of 200, 500 and 1000. Figure 3 presents streamlines and circumferential velocity contours for $Re = 500$ and $S = 0$ and $S = 1$. Swirl-induced increases in entrainment are clearly visible when the streamlines are compared. Also of note is the thicker boundary layer for $S = 1$. As a consequence of this thickened boundary layer, and in agreement with the literature, increased swirl leads to a reduction in heat transfer. In addition, the surface pressure in the impingement region is substantially reduced.

Figure 4 illustrates the Nusselt number distribution on the lower wall due to varying swirl numbers. In agreement with the previous work of Huang *et al.* [3], small swirl number has minor influence on the Nusselt number distribution. As the imposed swirl approaches $S = 1$, much greater effects were observed. Indeed, the peak Nusselt number at $S = 1$ was reduced by approximately 34%. Because of the large area considered, the local values at the impingement point have somewhat less influence on the average Nusselt

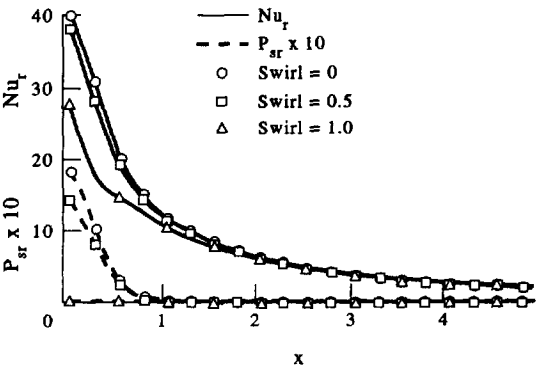

Fig. 4. Local Nusselt number and nondimensional surface pressure distribution for an impinging jet at $Re = 500$.

number. Consequently, this large reduction at the impingement point led to only a 3.3% drop in the average Nusselt number. However, since the impingement point pressure played a larger role in the average pressure, the 78% local reduction led to a 48% reduction in the total surface pressure for $S = 1$.

Both of these effects can be explained by noting the increased entrainment of the quiescent fluid into the jet. This leads to decay in jet speed and a consequent reduction in the pressure force on the impingement surface. At $Re = 500$ and $S = 0$, the ratio of fluid entrained into the cavity to fluid injected through the axial jet is found to be 1.69. This ratio increased slowly with increasing swirl to a value of 1.81 at $S = 1.0$.

It may be mentioned that in one of the earlier studies [9] in the related area the numerical result for the pure axial jet (without superimposed swirl) was compared favourably with the results of Deshpande and Vaishnav [10].

Radial jets

The radial jet considered here has a nondimensional radius of 0.5, an exit width of 0.5 and is positioned

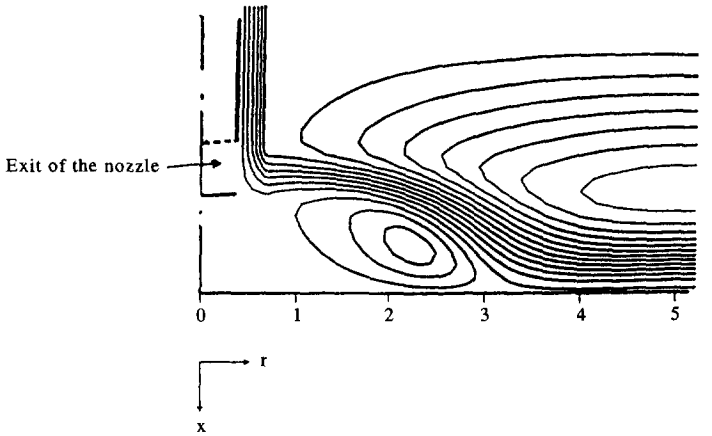

Fig. 5. Radial jet streamlines with $Re = 500$.

such that the center of the jet exit is located at 1.25 nondimensional units above the impingement surface. As with the axial jet, the partially confined domain of $H = 3$ and $L = 5$ encloses the radial jet. A parabolic entrance profile, which issues at an angle $\vartheta = 0°$ from the jet exit normal (positive downward), has been assumed. A typical flow field, at $Re = 500$, is illustrated by Fig. 5.

In order to examine the effect of the upper wall on the quantities of interest, a test was performed in which the cavity height was doubled to a nondimensional value of 6. Curiously, under standard conditions, the upper wall had very little influence on either the heat transfer or the reattachment point. However, the upper wall *can* have a very significant influence for high free convective effects and negative flow exit angles (where fluid emanates in the upward direction). The effects of free convection and jet inclination angle will be considered elsewhere.

Radial jet with swirl

As with the swirling axial jet, a solid-body rotational profile has been assumed at the jet exit; consequently, the circumferential velocity is given by $w = R\omega$. Simulations have been conducted at Reynolds numbers of 200, 500 and 1000 for swirl numbers ranging between 0 and 1.

A typical swirling radial jet and associated flow field, at $Re = 500$ and $S = 1.0$, is presented in Fig. 6. As illustrated here by the shading zone, a large amount of circumferential momentum has been injected into the flow field which has finally evolved into a boundary-layer-like 'wall swirl' along the impingement surface. Through comparison with Fig. 5, it becomes obvious that the location of the reattachment ring has moved significantly *towards* the axis of symmetry.

The circumferential velocity component leads to increased entrainment into the main flow stream. Such an entrainment has the effect of augmenting the so-called 'Coanda effect' by lowering the pressure in the recirculation zone. At $Re = 500$, this moves the reattachment point inwards, and possibly also contributes to increases in the transport coefficient. At $Re = 500$, the ratio of fluid entrained into the cavity to fluid injected through the jet rises from 1.37 to 3.16 as the swirl number is increased from 0 to 1.

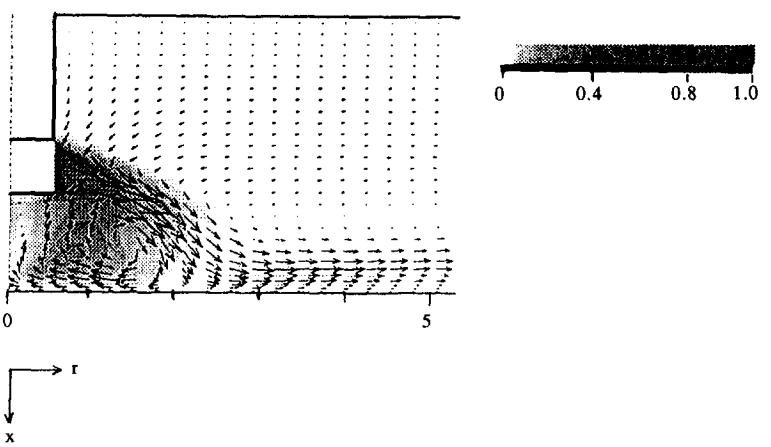

Fig. 6. Radial jet flow field with entrance swirl $S = 1$. Shaded regions indicate swirl velocity.

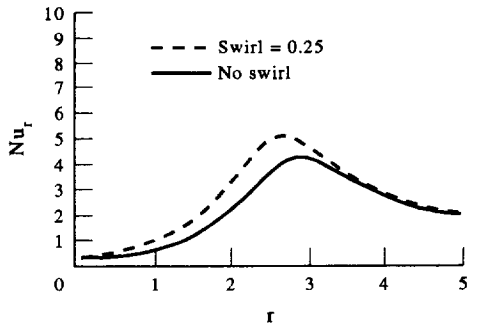

Fig. 7. Radial jet local Nusselt numbers at inclination angle $\vartheta = 0°$ for $Re = 500$.

In contrast to the transport coefficient reductions observed with axial jets, significant local and average Nusselt number increases can be obtained with swirling radial jets. The local effect of swirl on the Nusselt number distribution can be observed in Fig. 7, where results are presented for swirl numbers of zero and 0.25. In each of the cases, the value of the average heat transfer enhancement, relative to the no-swirl values is 12.0%.

Figure 8 shows the variation in average surface pressure and heat transfer coefficient with swirl for various Reynolds numbers. With increasing swirl number, the average Nusselt number increases significantly and the surface suction force is also increased. The percentage increase in heat transfer, relative to the no swirl case, varies with the Reynolds number; the total enhancement at $S = 1.0$ was 77% for the $Re = 200$ case, 66% at $Re = 500$ and 65% at $Re = 1000$. The nondimensional suction force increased strongly with swirl and Reynolds number. At $S = 1.0$ and $Re = 200$, 500 and 1000, surface suction relative to the $S = 0$ case increased by *factors* of 1.6, 6.6 and 11.9, respectively.

CONCLUSIONS

Laminar axial and radial jets respond very differently to the superimposed swirl. As noted in the literature, and confirmed in this study, the Nusselt number produced by an axial jet is always reduced by the superimposed swirl. However, as not previously noted, the impingement force directly under the nozzle exit can be greatly reduced by high levels of swirl, as can the average pressure force. Both the heat transfer and surface pressure reduction are caused by additional entrainment within the flow stream; however, the amount of external fluid entrained into the cavity does not rise dramatically with increasing swirl number.

In sharp contrast, the superimposed swirl on a radial jet results in a large rise in the average and local Nusselt numbers, the suction force, and the amount of external fluid entrained into the cavity.

The predicted increases in heat transfer at $S = 1.0$ reach as high as 77% for the $Re = 200$ case, 67% for $Re = 500$ and 66% at $Re = 1000$. These increases are accompanied by increases in the average suction by as much as a factor of 11.9. Significant enhancement is also observed at lower swirl numbers. Swirl as low as $S = 0.25$ can also improve overall heat transfer performance.

Since small amounts of swirl in axial jets do not greatly reduce heat transfer, it is probably not necessary to take extraordinary measures to minimize its occurance in most systems. In contrast, even small amounts of swirl can significantly increase heat transfer with radial jets. However, since any such increase incurs momentum losses, careful consideration should be taken before the application of swirl. In any case, such application should probably await experimental data.

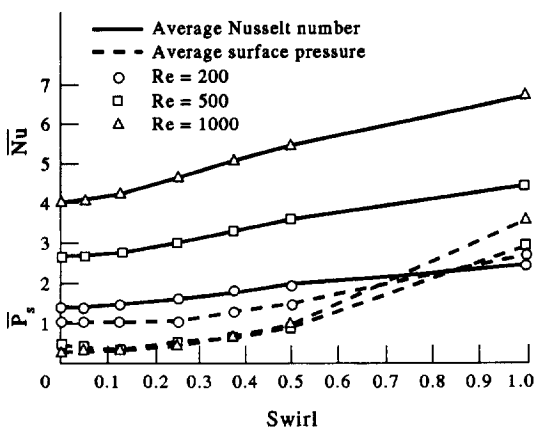

Fig. 8. Average Nusselt number and surface pressure for radial jets with Reynolds numbers of 200, 500 and 1000 as a function of entrance swirl.

Acknowledgement—This work has been supported by the Deutsche Forschungsgemeinschaft.

REFERENCES

1. R. Viskanta, Heat transfer to impinging isothermal gas flame jets, *Expl Thermal Fluid Sci.* **6,** 111–134 (1993).
2. C. Ostowari, B. Paikert and R. H. Page, Heat transfer measurement of radial jet reattachment on a flat plate, presented at *National Fluid Dynamics Congress*, Cincinnati, 25–28 July (1988).
3. J. M. Beer and N. S. Chigier, *Combustion Aerodynamics*. Applied Science, London (1972).
4. B. Huang, W. J. M. Douglas and A. S. Mujumdar, Heat transfer under a laminar, swirling impinging jet—a numerical study, *Proceedings of the Sixth International Heat Transfer Conference*, Vol. 5, pp. 311–316. Hemisphere, Washington, DC (1978).
5. J. Ward and M. Mahmood, Heat transfer from a turbulent, swirling, impinging jet, *Proceedings of the Seventh International Heat Transfer Conference*, Vol. 3, pp. 401–407. Hemisphere, Washington, DC (1982).
6. J. Ward and M. Mahmood, *The Effect of Swirl on Mass/heat Transfer from Arrays of Turbulent, Impinging Jets*, ASME-WAM, HTD-Vol. 256, pp. 57–64. ASME, New York (1993).
7. J. Kim and P. Moin, Application of a fractional-step method to incompressible Navier–Stokes equations, *J. Comput. Phys.* **59,** 308–323 (1985).

8. H. Laschefski, D. Braess, H. Haneke and N. K. Mitra, Numerical investigations of radial jet reattachment flows, *Int. J. Numer. Meth. Fluids* **18,** 629–646 (1994).
9. S. Chakraborty, S. P. Sengupta and G. Biswas, Fluid flow and heat transfer in a laminar radial impinging jet, *Int. J. Numer. Meth. Heat Fluid Flow*, **4,** 173–185 (1994).
10. M. D. Deshpande and R. N. Vaishnav, Submerged laminar jet impingement on a plane, *J. Fluid Mech.* **114,** 213–236 (1982).